Received: 27 April 2018 | Revised: 22 August 2018 | Accepted: 29 September 2018

DOI: 10.1111/jace.16146

ORIGINAL ARTICLE

Journal of the American Ceramic Society

Planetary ball-milling of AlON powder for highly transparent ceramics

Zhao Feng[1,2] | Jianqi Qi[1,3] | Xu Huang[1] | Xiaofeng Guo[4,5] | Yin Yu[6] | Xiuxia Cao[6] | Yuezhong Wang[7] | Di Wu[5,8] | Chuanmin Meng[6] | Tiecheng Lu[1,2,3]

[1]College of Physical Science and Technology, Sichuan University, Chengdu, China

[2]Key Laboratory of Radiation Physics and Technology of Ministry of Education, Sichuan University, Chengdu, China

[3]Key Laboratory of High Energy Density Physics of Ministry of Education, Sichuan University, Chengdu, China

[4]Department of Chemistry, Washington State University, Pullman, Washington

[5]Alexandra Navrotsky Institute for Experimental Thermodynamics, Washington State University, Pullman, Washington

[6]Institute of Fluid Physics, Key Laboratory of Shock Wave and Detonation Physics, Mianyang, China

[7]Tianjin Key Laboratory of Optical Thin Film, Tianjin Jinhang Technical Physics Institute, Tianjin, China

[8]The Gene and Linda Voiland School of Chemical Engineering and Bioengineering, Washington State University, Pullman, Washington

Correspondence
Jianqi Qi and Tiecheng Lu, College of Physical Science and Technology, Sichuan University, Chengdu, China.
Emails: qijianqi@scu.edu.cn (JQ) and lutiecheng@scu.edu.cn (TL)

Funding information
Key Applied Basic Research of Sichuan Province, Grant/Award Number: 2017JY0329; The Science and Technology Innovation Team of Sichuan Province, Grant/Award Number: 15CXTD0025; National Science Foundation of China (NSFC), Grant/Award Number: 1602244, 11602245, 51702231; Foundation of National Key Laboratory of Shock Wave and Detonation Physics, Grant/Award Number: 9140C670302160C07001; NSAF, Grant/Award Number: U1830136

Abstract

A detailed investigation of planetary ball-milling for coarsened AlON powder was carried out. Our results showed that the weight ratios of milling ball-to-powder, the revolution rate and the planetary ball-milling time have significant impacts on the microscopic morphology, particle size distribution and average particle size of powder. The process and mechanism were analyzed, and the outcome of our study can be used to optimize the complicated planetary ball-milling method by controlling the planetary ball-milling time or adjusting the revolution rate at the final stage of planetary ball-milling. Sequentially, using fine and uniform AlON powder by optimized planetary ball-milling with an average particle size below 300 nm and excellent sintering properties, highly transparent AlON ceramic with an in-line transmittance of 84% at 2000 nm was successfully prepared through pressureless sintering at 1880°C for 6 hours using the elaborative treated powder synthesized from carbothermal nitridation method.

KEYWORDS
particle size distribution, planetary ball-milling, transparent AlON ceramic

1 | INTRODUCTION

Transparent aluminum oxynitride ceramic (γ-AlON) is one of the most useful ceramic materials that attracts broadening interests in many fields due to its excellent physical and chemical properties. Its superior hardness and strength, high transparency, and high corrosion-resistance properties make γ-AlON a good candidate for transparent armors, infrared window, domes, and phosphors.[1–4] Traditionally, transparent AlON ceramic is prepared by the following procedures: synthesizing and milling of powder, then shaping of green body and followed by the sintering of the ceramic. Synthesis methods include solid-state reaction method,[5,6] aluminothermic reduction nitridation method,[7,8] and carbothermal nitridation method (CRN).[9,10] The synthetic AlON powder can be sintered into ceramics by hot-

pressing method,[11,12] hot isostatic pressing method,[13,14] and pressurless sintering method.[15,16] Particularly, combing carbothermal nitridation method with pressurless sintering method is preferred due to its low cost, which enables potential commercialization with large-scale production for highly transparent AlON ceramics.

AlON powders synthesized from CRN method usually feature large grain size and hard agglomeration due to its high synthesis temperature (above 1700°C). Those coarse powders compromise the sintering ability of powder severely that they cannot be used to fabricate highly transparent ceramic directly. Moreover, coarse pores of those CRN method-synthesized powders universally present not only between but also inside the grains. The intracrystalline pores are difficult to remove during the pressureless sintering because the removal is mainly controlled by kinetics instead of thermodynamics.[17,18] In contrast, smaller particle-size favors the promotion of the densification rate of sintering[19–22] by improving the surface diffusion through which the mass transport significantly contributes to the densification especially in the initial and intermediate stages of sintering.[18,23] Therefore, the key to a fast fabrication of highly transparent AlON ceramic is to obtain highly pure and dispersed powder with small average particle size (APS) and narrow particle size distribution (PSD). Multiple methodologies are employed to enable this objective, for instance, ball milling,[24–26] optimized CRN method using core-shell structured Al_2O_3/C as raw powders.[27]

However, as far as we know, none of these studies on planetary ball-milling method of AlON powder clearly reveal the mechanistic systematics. Shan et al[24] used Si_3N_4 balls with the diameter of 5, 8, and 10 mm, with weight ratio of 1.7, 1, and 1.3, respectively, for planetary ball-milling media. The weight ratios of ball-to-powder, and alcohol to powder are 7, and 3.93, respectively. After planetary ball-milling for 24 hours at 170 R/min, bimodal PSD fine powders at 1.1 and 2.2 μm were obtained and used for fabricating highly transparent ceramics with the fast pressureless sintering method. Liu et al[16] prolonged the planetary ball-milling time of AlON powders to 24 hours at 130 R/min, resulting in powders with an average particle size of 1.38 μm that can be further sintered into highly transparent AlON ceramics. Despite of being an effective method, the details of planetary ball-milling method are not usually given in previous studies,[25,26,28,29] and planetary ball-milling received little systematic studies on the mechanism and controlling parameters while employed in processing AlON powders.

In this work, AlON powders were synthesized by CRN method and then treated by planetary ball-milling. We carefully investigated the effects of ball-to-powder weight ratio, revolution rate and time of planetary ball-milling on the microstructures, morphology, APS, PSD, phase assemblage of AlON powders, and the optical properties of AlON ceramics. Particularly, the mechanism of how the planetary ball-milling method affects the quality of final powder as a function of treatment time was discussed. With an understanding of the role of planetary ball-milling time, merely by controlling the time, we were able to produce AlON powders with desired PSD and APS. These powders can then be fabricated by the fast pressureless sintering method to reliably produce highly transparent AlON ceramics.

2 | EXPERIMENTAL PROCEDURE

Solid starting materials are 472.50 g high purity γ-Al_2O_3 (99.99%, UPC818; Zhejiang Ultrafine Powder & Chemicals co., Ltd., Zhejiang. China) and 27.50 g carbon black (99.9%, M880; Cabot Chemical Co., Ltd., Tianjin, China). The materials were placed into a nylon jar with alumina balls (3.7 g/cm^3, Φ10 mm, Jingdezhen Betterwear New Materials Co., Ltd., Zhejiang. China) and then mixed with 900 mL absolute ethyl alcohol for 8 hours by a horizontal ball grinder. After removing the balls, the obtained slurry was dried at 70°C for 48 hours. Then the dried mixtures were screened through a 140-mesh nylon sieve (Table 1).

The mixture powder (γ-Al_2O_3 and carbon black) was loaded into a graphite crucible which was placed in a vertical graphite furnace flushed by 0.5 L/min of high purity nitrogen under 1 atm. First, the mixture powder was heated to 1550°C with a heating rate of 10°C/min and dwelled for 2 hours to synthesize the Al_2O_3—AlN composites as the intermediate products. Then the temperature was raised to 1750°C with a heating rate of 5°C/min and hold for another 2 hours to obtain the final product, single-phase AlON powder. Finally, this AlON powder was calcined at 650°C for 10 hours in air to burn out any residual carbon or graphite.

In total, 750 g of single-phase AlON powder was synthesized by the carbothermal reduction and nitridation (CRN) method. All the powder was divided into 15 batches equally (50 g each batch), for the following study of planetary ball-milling method. One vertical planetary ball-milling grinder with a constant ratio of 2:1 of rotating rated of the jar and sun disk was used in this study. To control the degree of contamination introduced by the milling-balls, high quality alumina balls (3.7 g/cm^3, Φ5 mm, Jingdezhen Betterwear New Materials Co., Ltd., Zhejiang. China), and nylon jar were used in our study. The goal of this work is to gain the AlON powder with the average particle size below 500 nm, thus, each batch with 50 g powder and 100 mL absolute ethyl alcohol to form the slurry with a good fluidity. For that reason, the ratio of absolute ethyl alcohol to powder is kept at 100 mL/50 g for all the samples.

TABLE 1 Parameters in planetary ball-milling of AlON powder

	Ball (g)	Powder (g)	Alcohol (mL)	Revolution rate (R/min)
$W_{2.5}$	125	50	100	200
W_5	250	50	100	200
W_{10}	500	50	100	200
R_{150}	500	50	100	150
R_{250}	500	50	100	250

First, the effects of weight ratios of ball-to-powder on the PSD and APS of powder were studied through samples with different weight ratios of ball/powder = 2.5, 5, and 10, labeled as $W_{2.5}$, W_5, and W_{10}, respectively. Second, after the sample being screened that has the appropriate weight ratio of ball-to-powder, it was then ball-milled at different revolution rate of 150 and 250 R/min, labeled as R_{150} and R_{250}, respectively, to study the effects of the revolution rate on PSD and APS of powder. At last, with an appropriate weight ratio and revolution rate, we performed study on the effects of planetary ball-milling time on the morphology, phase assemblage, PSD and APS of powder. Powder resulted from planetary ball-milling for 0, 10, 15, 20, 25, 30, 35, 40, and 45 hours were labeled as T_0, T_{10}, T_{15}, T_{20}, T_{25}, T_{30}, T_{35}, T_{40}, and T_{45}, respectively. The soft agglomeration occurred during planetary ball-milling process was also studied by changing the revolution rate at the final stage of planetary ball-milling (sample $R_{225+125}$).

In addition, to study the effects of planetary ball-milling time on the transparency of AlON ceramics, samples T_{15}, T_{25}, T_{35}, and T_{45}, were chosen and mixed with 0.05 wt % Y_2O_3 and 0.2 wt % MgO as sintering agents homogeneously in absolute alcohol by planetary ball-milling method at 150 R/min for 5 hours, and then dried at 70°C for 48 hours. Four groups of pellets, were prepared by uniaxial pressing the corresponding powder into 20 mm diameter stainless steel die at 10 MPa, and then followed by the cold isostatic pressing treatment at 200 MPa. Those AlON green bodies were firstly heated in a vertical vacuum graphite furnace at 200°C for 2 hours to remove any absorbed water in the green bodies and then filled the graphite furnace with 0.1 MPa flowing high purity nitrogen of 0.1 L/min. The temperature was then raised to 1880°C with a heating rate of 10°C/min and dwelled for 6 hours, followed by a cooling to room temperature with a rate of 15°C/min. Finally, the sintered samples of AlON ceramics were ground and mirror polished on both sides to a thickness of 1.5 mm for optical property measurement.

The morphologies of AlON powder and ceramics were examined by a field emission scanning electron microscope (FE-SEM; s-4800; Hitachi, Tokyo, Japan). The PSD of AlON powders were measured by laser size analyzer (Model Mastersizer 3000; Malvern, Malvern, UK). The phase assemblage of AlON powder was determined by X-ray diffractometer (XRD; DX-2700; Dandong Fangyuan, Dandong, Liaoning, China) using nickel-filtered Cu$K\alpha_1$ radiation (λ = 1.5406 Å). The optical in-line transmittances of the AlON ceramics were recorded over the wavelength range from 200 to 2000 nm by an UV-vis-NIR spectrophotometer (Lambda-750; Perkin-Elmer, Waltham, MA, USA).

3 | RESULTS AND DISCUSSION

3.1 | Effects of weight ratios of milling ball-to-powder and the revolution rate on the morphology, PSD and APS of powder

As shown in Figure 1, the particle size of AlON powders exhibits a clear decreasing trend with respective to the increase in weight ratio of milling ball-to-powder and the revolution rate. It is seen from Figure 1A that the PSD of sample $W_{2.5}$ is not uniform with particle size ranging from ~0.5 to ~5 μm. Such low weight ratio produced breakages of the sintering necks between grains and little agglomeration**.** Figure 1B shows the morphology and PSD of powder from sample W_5. Although the weight ratio is doubled, no agglomeration and particles larger than 2 μm are found from the SEM, but the PSD is much more uniform compared with sample $W_{2.5}$ (Figure 2A). As the weight ratio increases to 10, for sample W_{10}, fine and uniform particles are obtained. We also investigated the effects of revolution rate. Specifically, sample R_{150}, sample R_{250}, and sample W_{10} vary as revolution rate evolves (see Figure 2A-C). After ball milling for 24 hours, at a constant weight ratio of ball-to-powder (500/50) and 150 R/min, no detectable large particles were found in the SEM (Figure 1A)**.** Finer and more uniform particles are gained when the revolution rate increased to 250 R/min.

To make a clear comparison, Figure 3 shows the changes of the PSD and APS respect to the weight ratios and revolution rates, also the changes of D_{10}, D_{90} are shown in the insets. It is clearly shown that with the increase in weight ratio of milling ball-to-powder, the peak of PSD moves to smaller particle size field (Figure 3A), and the D_{10}, D_{90} and APS decrease (Figure 3B). Particularly, the D_{10}, D_{90}, and APS decrease more steeply from weight ratio of 2.5~5 to 5~10, suggesting approaching a plateau beyond which increasing the weight ratio will have minimal impacts. Thus, we conclude that 10 is the optimized weight ratio of milling ball-to-powder ratio. The impact of changing revolution rate can be clearly seen in Figure 3C,D. The peak of PSD shifts to smaller particle size field gradually and the APS decrease almost linearly with the increase in revolution rate. Considering the values of D_{10}, D_{90} are small and the APS is already below 500 nm and high revolution rate introducing more impurity, the suitable revolution rate may about 250 R/min and no need to increase the revolution rate any more.

3.2 | Effects of ball milling time on the morphology, PSD and APS, phase assemblage of powder

Other than the weight ratio of milling ball-to-powder and the revolution rate in the planetary ball-milling method for AlON, the ball milling time is another important factor. During this investigation, the planetary ball-milling revolution rate was slow down to 225 R/min to further decrease the impurities introduced by the milling balls, and the weight ratio of milling ball-to-powder was 500/50. The results are shown in Figures 4-6.

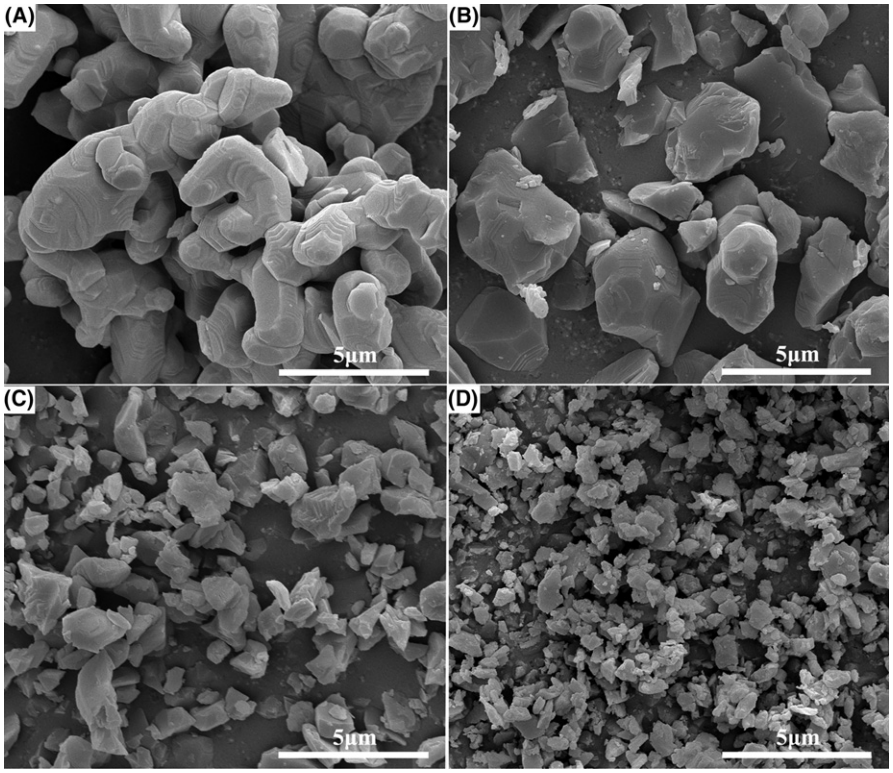

FIGURE 1 Morphology of un-ball-milled (A), and ball-milled AlON powder: (B) sample $W_{2.5}$, the ratio of milling ball-to-powder is 125/50 and the revolution rate is 200 R/min, (C) sample W_5, the ratio of milling ball-to-powder is 250/50 and the revolution rate is 200 R/min, (D) sample W_{10}, the ratio of milling ball-to-powder is 500/50 and the revolution rate is 200 R/min

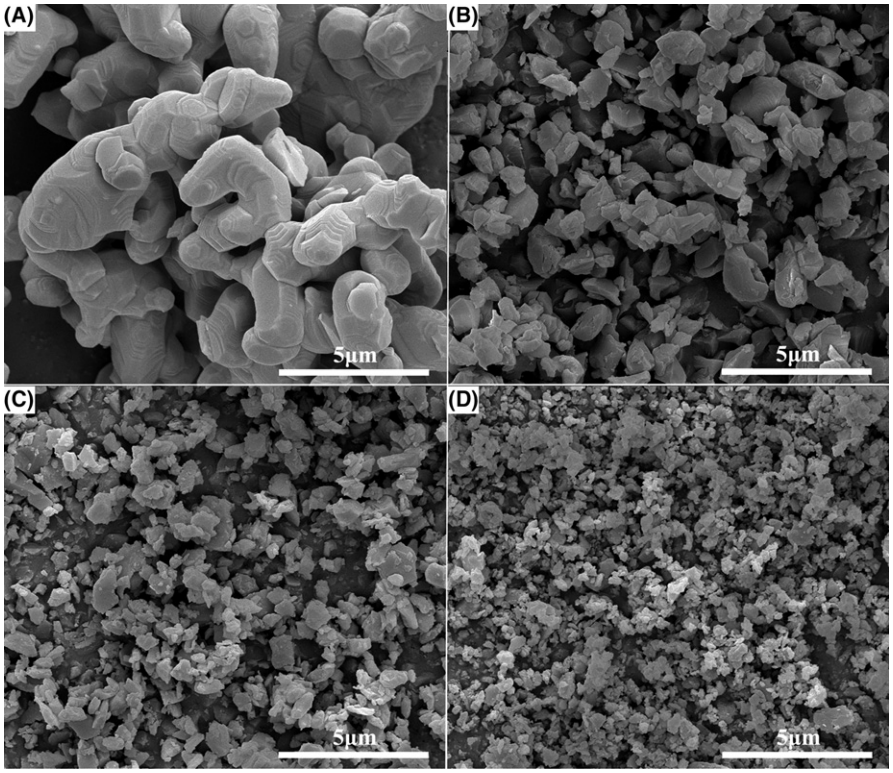

FIGURE 2 Morphology of un-ball-milled (A), and ball-milled AlON powder: (B) sample R_{150}, the ratio of milling ball-to-powder is 500/50 and the revolution rate is 150 R/min, (C) sample W_{10}, the ratio of milling ball-to-powder is 500/50 and the revolution rate is 200 R/min (D) sample R_{250}, the ratio of milling ball-to-powder is 500/50 and the revolution rate is 250 R/min

As shown in Figure 4A, the as-synthesized AlON powder exhibits severe hard agglomerations and irregular coarse morphology. After ball milled for 10 hours (Figure 4B), the particle size decreases significantly and there is no large or hard agglomerations observed. However, the PSD is still not uniform that smaller particles absorb onto the bigger ones, seen in the inset SEM photo of Figure 4B. As the ball milling time increases, the particle size of powder gradually decreases and the PSD becomes more uniform (Figure 4B-I). When the ball milling time reaches 20 hours, the particle size decreases to submicron scale and absorb onto each other forming soft agglomerations (Figure 4D). Further increasing the ball milling time to 25~45 hours does not decrease APS or improve PSD obviously, as seen in Figure 4.

Clearly, in Figure 5A, with the increase in ball-milling time, the peak of PSD firstly moves to smaller size region and then shifts back to larger size region, due to the soft agglomeration occurred during the ball milling process as showin in Figure 4E-I. Figure 6A shows the relationship of D_{10}, D_{90} as ball-milling time varies. Both D_{10} and D_{90} show a tendency of decrease followed by increasing as the ball-milling time increases. To further study the relationship between particle size and ball-milling time, APS data were also plotted against ball-milling time, as shown in Figure 6B. The curve fitted based on the experimental data shows a shape of "V" with the ball-milling time from 0 to 40 hours. Both the PSD profiles and the minimum in the "V" suggest 20 hours as ball milling-time is an optimal condition for obtaining AlON powder with a smallest APS (316 nm) and a narrowest PSD. Having concluded that 20 hours may be the most suitable ball-milling time for our work, small particle size and low soft agglomeration powder can still be obtained by combining the fast and low revolution rate, just as the result of sample $R_{225+125}$.

As shown in Figure 7, the diffraction peaks in the XRD pattern of ball milled AlON powder shows a trend of broadening with the prolongation of ball-milling time, suggesting the

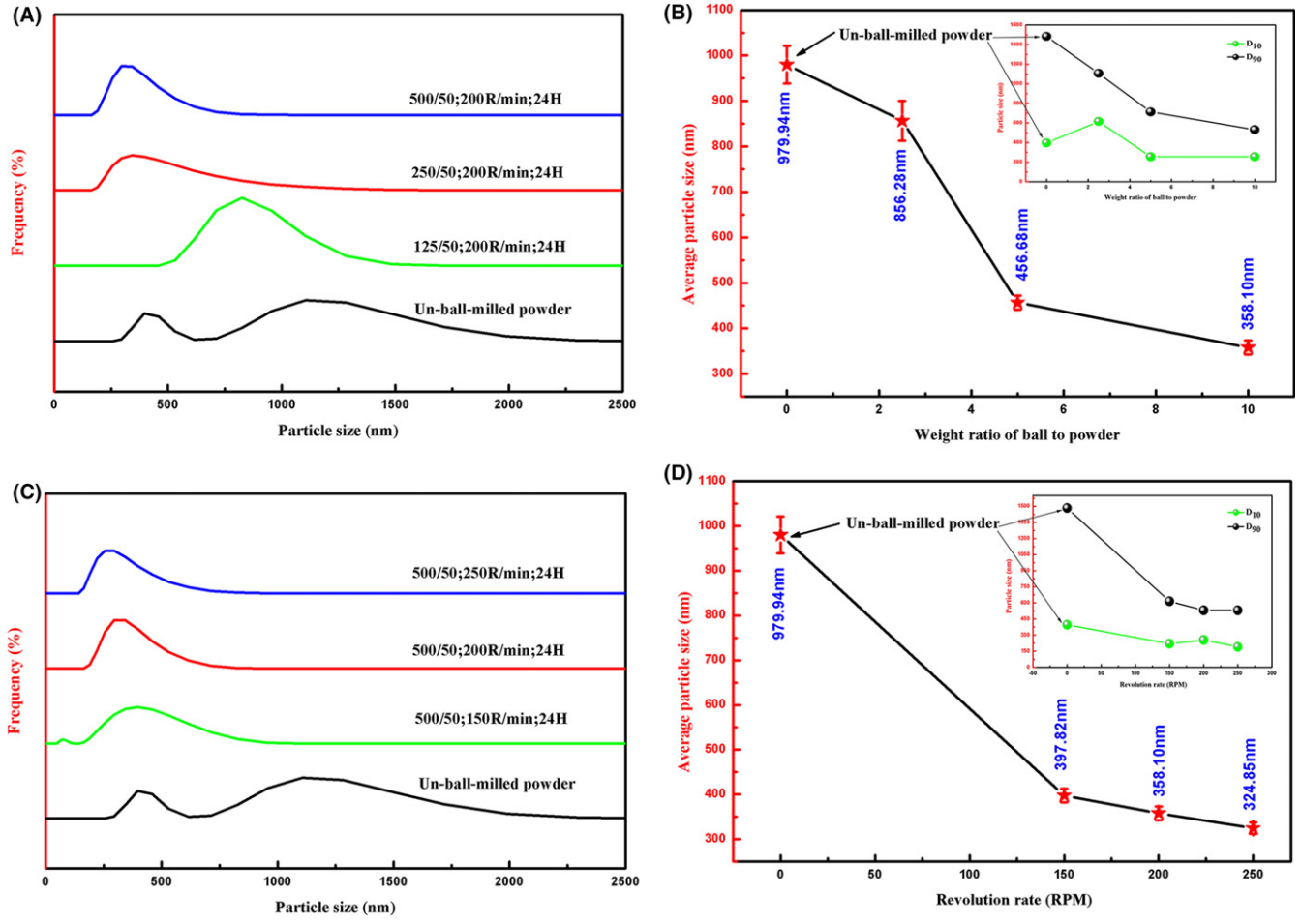

FIGURE 3 Particle size distribution and average sizes of un-ball-milled AlON powder, and AlON powder ball-milled with different parameters: A, particle size distribution of different ratios of milling ball-to-powder; B, the relationship of average particle size and the ratios of milling ball-to-powder (the inset figure is the relationship of D_{10}, D_{90} with the ratios of milling ball-to-powder); C, particle size distribution of different revolution rates; D, the relationship of average particle size and the revolution rate (the inset figure is the relationship of D_{10}, D_{90} with the revolution rate) [Color figure can be viewed at wileyonlinelibrary.com]

decrease in grain size. Also, the XRD pattern shows a pure cubic phase of AlON without any impurity phases of AlN or Al_2O_3 emerged during ball-milling process, which is a good indication that ball milling does not alter the structure of AlON or introduce significant amount of Al_2O_3. On the other hand, we used Al_2O_3 milling balls based on that AlON is a solid solution of AlN—Al_2O_3. In other words, AlON has the ability of assimilating some "impurity" Al_2O_3, which can be expressed as follows:

$$Al_{(64+x)/3}\square_{(8-x)/3}O_{32-x}N_x + Al_2O_3 \rightarrow Al_{(64+x')/3}\square_{(8-x')/3}O_{32-x'}N_{x'}. \quad (1)$$

Equation (1) is based on the simple model for AlON suggested by McCauley.[30] Where □ is cation vacancy, and x reflects the degree of N in AlON. Hence, considering this, small amount of Al_2O_3 introduced by milling balls is not the impurity for AlON powder. High-temperature sintering procedure of AlON ceramics will incorporate the small amount of Al_2O_3 into AlON with merely slightly modified x value.

3.3 | Mechanism of planetary ball-milling

planetary ball-milling is a very complicated process of powder pretreatment with multiple parameters, such as revolution, rotation rate and their semidiameters; material and density of milling ball, chosen solvent; weight ratio of milling ball/solvent/powder, ball-milling time and etc., controlling the characteristics of final powder products such as purity, morphology, agglomeration, PSD, and APS etc. Specifically, the purity level can be tuned by slection of

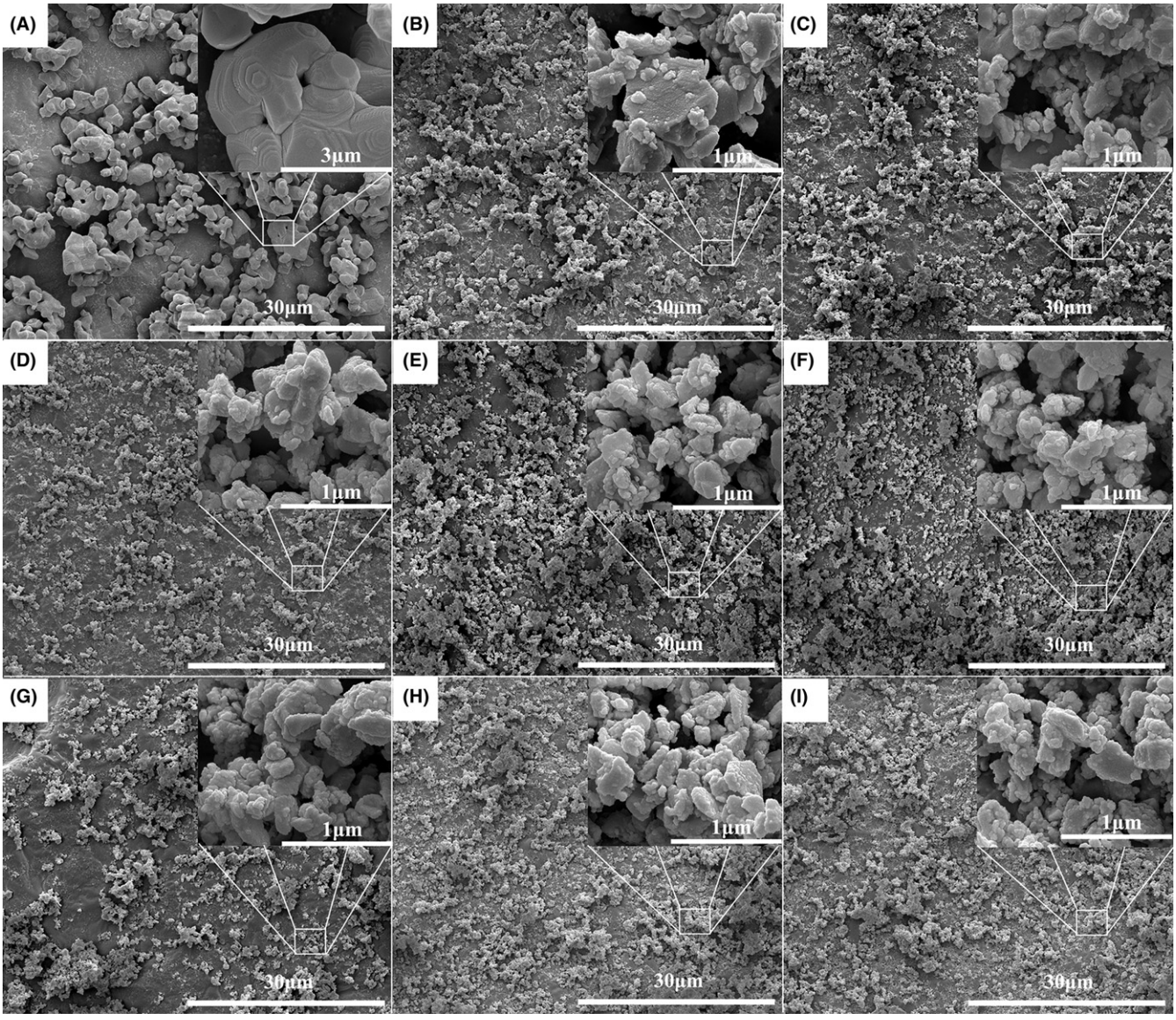

FIGURE 4 Morphology of A, as-synthesized; B, 10 h; C, 15 h; D, 20 h; E, 25 h; F, 30 h; G, 35 h; H, 40 h; I, 45 h ball milled AlON powders

the material of milling ball, the revolution and rotation rate and their semidiameters. To minimize the impurity introduced by the planetary ball-milling process, it is better to choose the ball consisting of same or similar materials as the milled powder, while mill running at possibly low revolution and rotation rate.

Consider Equation (2) to evaluate the impacts of the weight ratio of milling ball/powder on the morphology, PSD and APS, where $S_{\text{effective}}$ is the effective area, N is the total number of milling balls, and ΔS is the contact area between milling balls. The milling balls are arrayed as shown by Figure 8 to simplify our study. $S_{\text{effective}}$ can then be expressed as follows:

$$S_{\text{effective}} = 2 \times (N^{1/3} - 1)N^{2/3} \times \Delta S \quad (N = n^3, n \geq 2). \quad (2)$$

On the other hand, only increasing the number of milling balls enlarges $S_{\text{effective}}$ effectively, but does not improve the efficiency, $\eta_{\text{effective}}$, determinately. This is because that the efficiency also depends strongly on the weight ratio of solvent to powder, which can be expressed mathematically in Equation (4) by introducing the particle number density, n. Considering these two aspects, we can deduce the following:

$$\eta_{\text{effective}} \propto S_{\text{effective}} \quad (3)$$

$$\eta_{\text{effective}} \propto n. \quad (4)$$

Assume one particle is successfully milled by balls as a random generation event, and then the probability, P_{pb} of a random generation event has an intrinsically positive

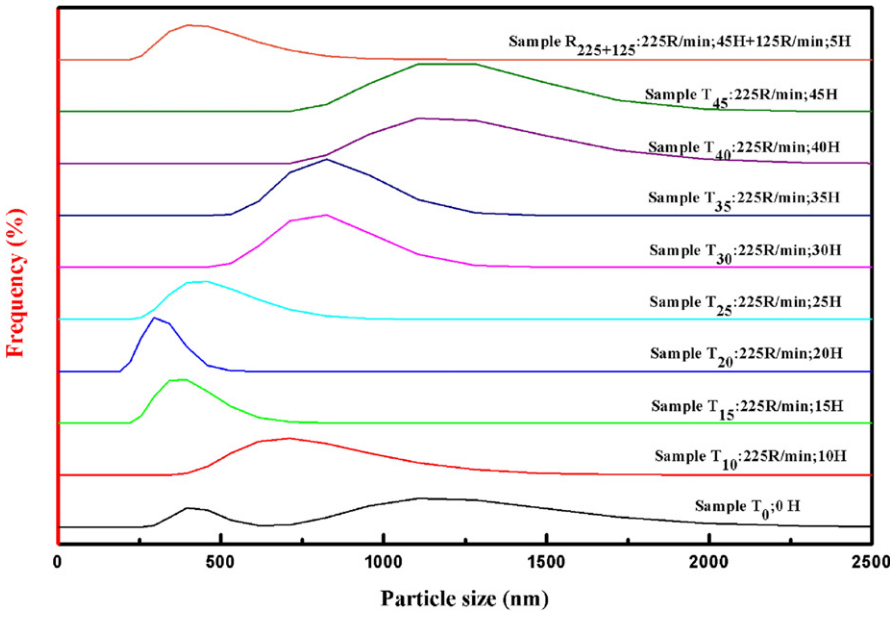

FIGURE 5 Particle size distributions of different ball-milling time [Color figure can be viewed at wileyonlinelibrary.com]

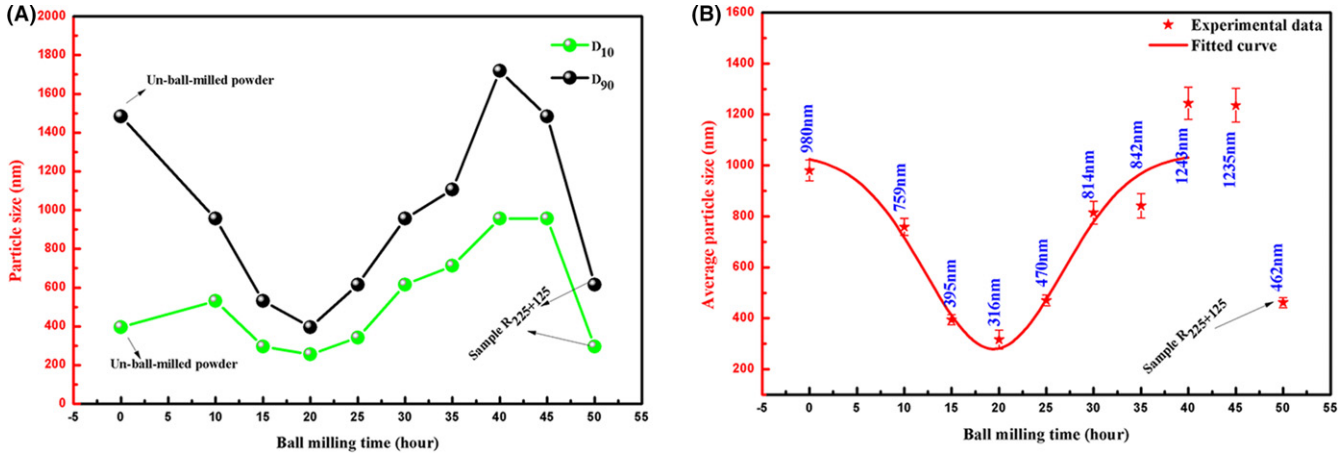

FIGURE 6 The relationship of (A) D_{10}, D_{90}, (B) average particle size with ball-milling time [Color figure can be viewed at wileyonlinelibrary.com]

correlation with the effective area of milling balls, $S_{effective}$. Thus, we can obtain Equation (3) showing the relationship of $\eta_{effective}$ and $S_{effective}$. Similarly, we assume milling balls successfully crushing particles as random generation events, and then the probability, P_{bp}, of a random generation event has a positive correlation with $\eta_{effective}$. Obviously, the denser the particle number (higher n), the higher is the probability P_{bp}, so the particle number n correlates the $\eta_{effective}$ positively, as seen in Equation 4.

Variances of densities of milling ball, the revolution and rotation rates, and semidiameters also have impacts on the morphology, PSD, and APS of the final powder due to the changes of the shear force, f_{shear}, the impact and pressure force, $f_{impact\ and\ pressure}$ provided by the energy: E of milling ball which can be expressed as follows:

$$E = \frac{1}{2}mv^2 + E_g, \tag{5}$$

where m and v are the mass and velocity of the milling ball, respectively, E_g is the gravitational potential energy of the milling ball. Equation (5) implies that heavy milling ball at a high revolution rate and a rotation rates provides a high energy for crushing the powder.

We can apply Equations (2-5) on understanding the experimental results of planetary ball-milling. At constant parameters such as the amount of absolute ethyl alcohol and powder and the revolution rate, the increase in $S_{effective}$ of milling balls (namely N of the milling balls in a certain volume) improves the efficiency: $\eta_{effective}$, which we observe in the experimental results shown in Figure 2A-C. The improvement of the efficiency can also be achieved by minimizing the weight ratio of absolute ethyl alcohol to powder to maximize the density of particles, n, as long as there is a good fluidity of slurry during the planetary ball-milling. What is more, as increase in the kinetic energy provided by the milling ball improves the efficiency according to the Equation (5). This can be seen in Figure 2D-F that higher revolution rate yield powders with smaller APS and narrow PSD.

The processing time of planetary ball-milling, T, is discussed based on parameters of weight ratio of solvent

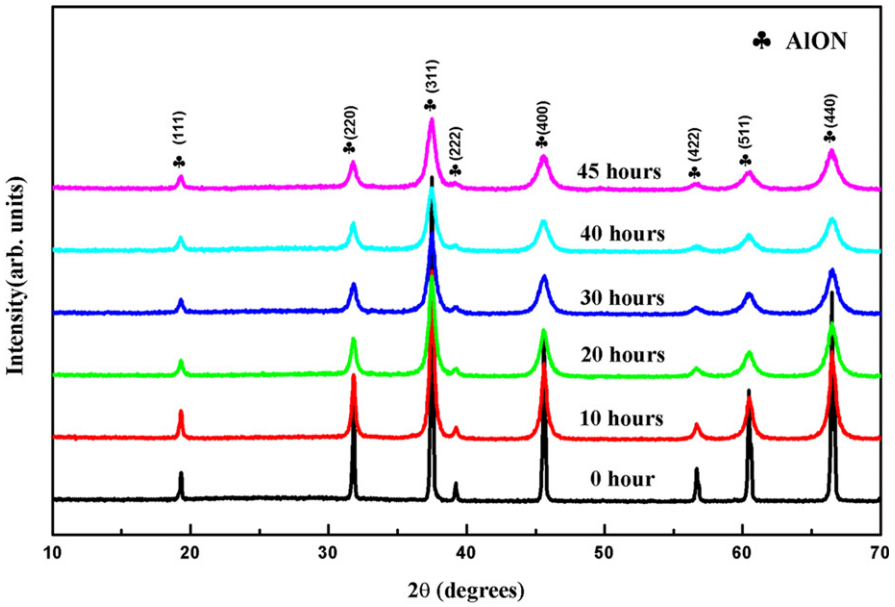

FIGURE 7 X-ray diffractometer pattern of AlON powder ball milled for different time [Color figure can be viewed at wileyonlinelibrary.com]

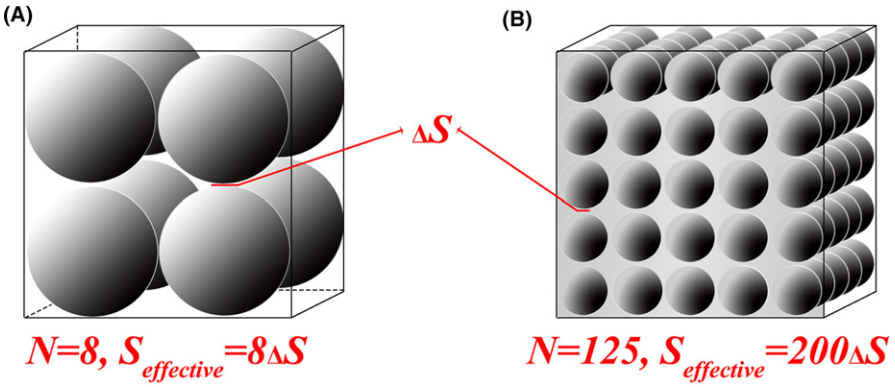

FIGURE 8 The relationship of effective area of milling balls: $S_{effective}$ and the number of milling balls: N [Color figure can be viewed at wileyonlinelibrary.com]

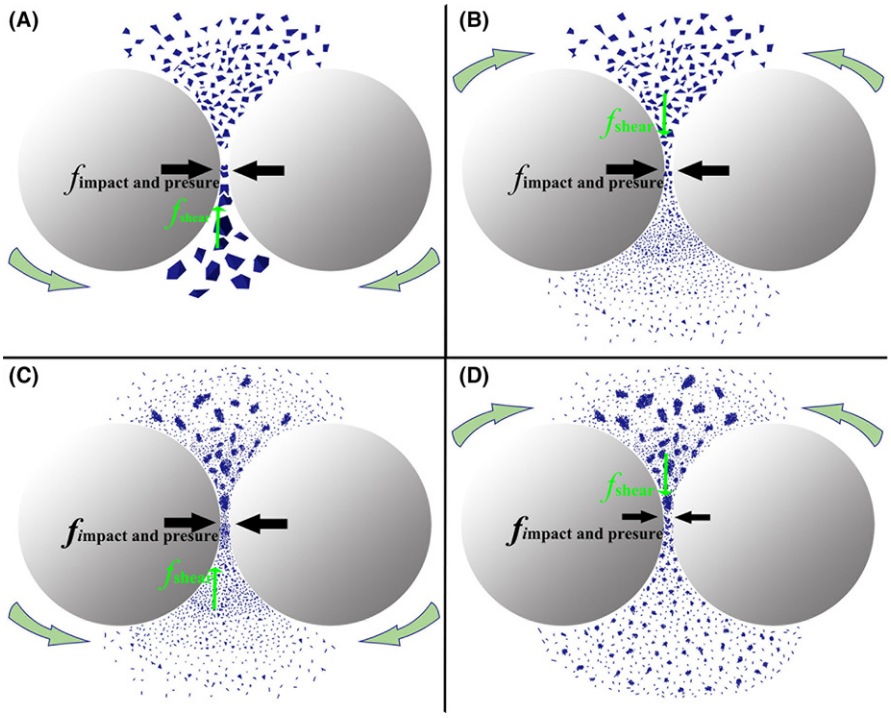

FIGURE 9 Stages of planetary ball-milling: A, large particles are crushed into smaller particles; B, refinement of smaller particles; C, agglomeration of fine particles; D, deagglomeration of fine particles at lower revolution rate [Color figure can be viewed at wileyonlinelibrary.com]

to powder, $S_{effective}$ and E are constant. The evolutions of PSD and APS of AlON during planetary ball-milling are shown in Figures 4 and 5 that suggest a non-linear impact from T on decreasing the APS of AlON powder. We divide the whole planetary ball-milling process into several stages, shown in Figure 9. In the first stage, Figure 9A, large particles are crushed into smaller particles by milling balls, and $f_{impact\ and\ pressure}$ provides most of the energy. In the next stage, Figure 9B, smaller particles are milled into fine particles and the PSD of powder gradually narrows, where both $f_{impact\ and\ pressure}$ and f_{shear} promote the refinement of particles. These two stages can be translated to the planetary ball-milling period of 0~20 hours as shown in Figures 4-6. In the third stage, Figure 9C, the planetary ball-milling method reaches its limitation, beyond which the prolongation of milling time actually increases APS due to the increase in the amount of finer particles that contributes to the agglomeration. This stage translates to the planetary ball-milling period of 25~45 hours. Therefore, we can conclude that the APS data collected by laser size analyzer is not the real APS of AlON powder. These three stages represent how planetary ball-milling time impacts the final powders with other parameters kept constant. However, since the agglomeration in slurry from stage 3 is caused by the relatively high surface energy and $f_{impact\ and\ pressure}$, we can deagglomerate the particles by slowing down the revolution rate. This is demonstrated by our sample $R_{225+125}$ that it is firstly milled for 45 hours at 225 R/min and then 125 R/min for 5 hours. A lower revolution rate decreases the effects of $f_{impact\ and\ pressure}$ on the agglomeration so f_{shear} can break the large agglomeration, shown in Figure 9D. The sample $R_{225+125}$ has its final APS decrease to 462 nm that prove our assumption.

Assuming parameters other than D (APS) and T (milling time) are constant, we also perform a fitting on the experiment data of the relationship of APS and T. the curve in Figure 6 based on the following equation (Gauss Amp Model):

$$D(T) = D_{\circ} + A \times \exp\left[-0.5 \times \left(\frac{T - T_C}{W}\right)^2\right], \quad (6)$$

where $D_{\circ}$ is the initial APS, A and W are constants which dependent on the experimental situation, respectively, the fitted equation is shown below:

$$D(T) = 1045 - 765\exp\left[-0.5\left(\frac{T - 20}{7}\right)^2\right](0 \le T \le 40). \quad (7)$$

Finally, after all the other parameters of planetary ball-milling are chosen reasonably, AlON powder with desired PSD and APS can be obtained easily by majorly controlling the ball-milling time, with adjusting the revolution rate at the final stage of ball milling if necessary.

3.4 | Microscopic morphology, phase assemblage, and transmittance of AlON ceramic

The microscopic morphology of AlON ceramic sintered from powder milled by planetary ball-milling method for different hours are shown in Figure 10. From Figure 10A,

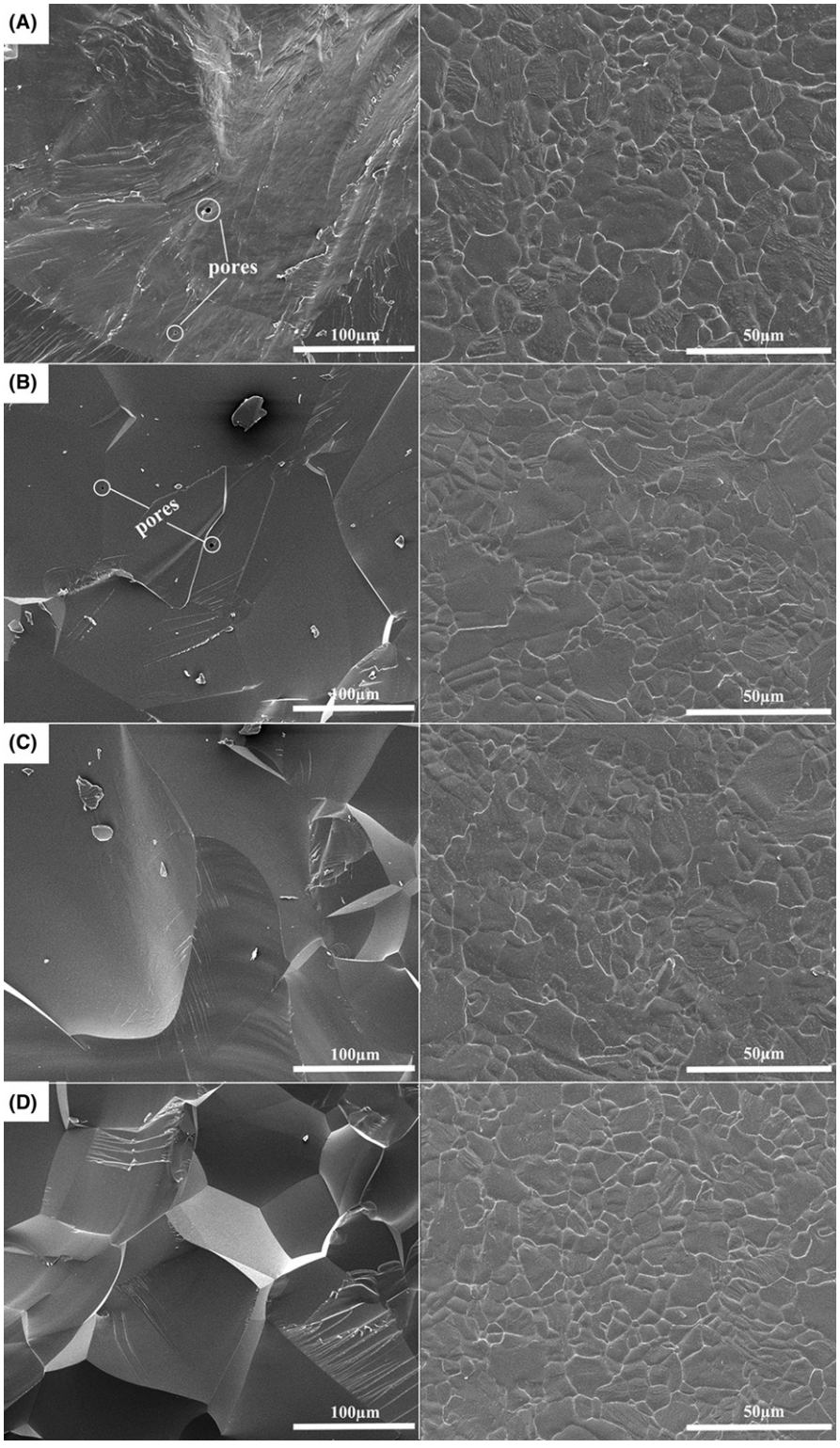

FIGURE 10 Fracture (left) and thermally etched (right) surfaces of AlON samples sintered from powder ball milled for: A, 15 h; B, 25 h; C, 35 h; D, 45 h

B, it can be seen that large pores with sizes from 1 to 3 μm are easily found between or in grains. Although in Figure 10C,D, the fracture surfaces are pore-free and clean which indicates a higher density of AlON ceramic body. The thermally etched surfaces give clear grain size distributions of AlON ceramic samples sintered from powder ball milling for different hours. The grain sizes of all the samples range from 10 to 40 μm and the size distributions become relatively more uniform when the planetary ball-milling time prolongates.

Figure 11 shows the XRD patterns of AlON ceramic sintered from powder ball milled for different time. Clearly, all the samples show a pure cubic phase of AlON and there is no impurity phases of AlN or Al_2O_3

found. Figure 12 shows the in-line transmittances and optical images of AlON samples sintered from powder ball milled for different time which exhibits a clear trend that the transmittances of AlON samples increase with the increase in planetary ball-milling time. Although the transmittance of sample sintered from 15 hours ball milled powder reaches 72% at the wavelength of 2000 nm, it has a strong dependence of the wavelength, indicating populated defects such as pores in the ceramic body as shown in Figure 10A. To the contrary, the in-line transmittance curve of sample sintered from powder ball milled for 45 hours shows much less dependence of wavelength from 400 to 2000 nm owing to its nearly full density ceramic body (Figure 10D). The transmittance also reaches 84% at the wavelength of 2000 nm that is higher than most of pressureless-sintered samples prepared by other researchers.[7,27–29]

4 | CONCLUSIONS

This study aimed at understanding the mechanism of one post-treatment method, the planetary ball-milling method, for coarsening AlON powder synthesized from carbothermal nitridation method. The effects of parameters (revolution rates, milling time, and the weight ratio of milling ball/powder/alcohol) on the morphology, particle size distribution and average particle size, phase assemblage of

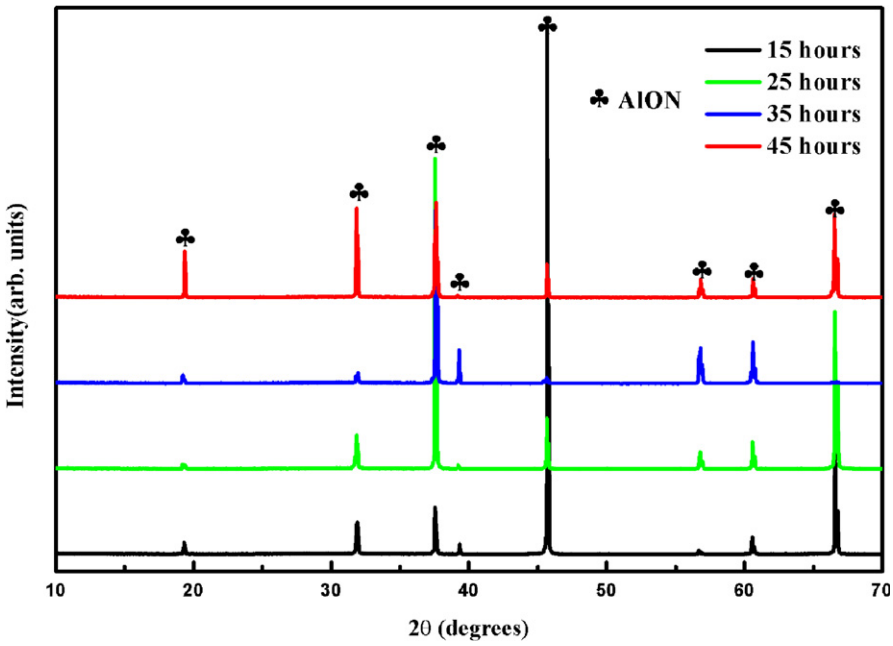

FIGURE 11 X-ray diffractometer pattern of AlON ceramic sintered from powder ball milled for different time [Color figure can be viewed at wileyonlinelibrary.com]

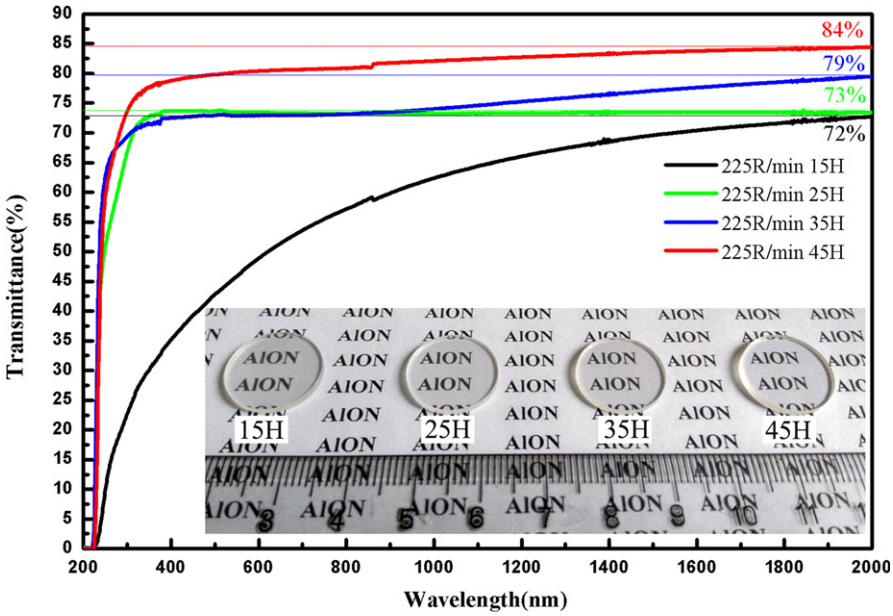

FIGURE 12 Transmittance curve of AlON ceramic sintered from powder ball milled for different time [Color figure can be viewed at wileyonlinelibrary.com]

final AlON powder were studied. The mechanism of planetary ball-milling method shows that the efficiency of milling has a strong relationship with the effective area of milling balls, the particle number density of powder, and the ball milling revolution rate. Optimal parameters are gained and simplified the complicated planetary ball-milling method to primarily control the ball milling time, and adjust the revolution rate if necessary. Based on our experiments, the planetary ball-milling process can be divided into three stages and the curve of the relationship of average particle size and ball-milling time present a "V" shape due to the agglomeration of particles in slurry. Agglomeration of particles is unavoidable in the planetary ball-milling process but the degree of agglomeration can be decreased by adjusting the ball-milling revolution rate. The effect of ball-milling time on the transmittance of AlON ceramic were studied and the result showed that transmittance increase with the prolongation of ball-milling time, which indicates that smaller average particle size and suitable particle size distribution are critical for preparing high transparent ceramics. Finally, high quality AlON powder was gained from the optimized planetary ball-milling process, and highly-transparent AlON ceramic with an in-line transmittance of 84% was prepared by pressureless sintering method.

ACKNOWLEDGMENTS

This work was supported by NSAF (No. U1830136), the Science and Technology Innovation Team of Sichuan Province (15CXTD0025), the Key Applied Basic Research of Sichuan province (2017JY0329), the National Natural Science Foundation of China (1602244, 11602245 and 51702231) and Foundation of National Key Laboratory of Shock Wave and Detonation Physics (9140C670302160C07001).

ORCID

Jianqi Qi http://orcid.org/0000-0002-6884-1258
Di Wu http://orcid.org/0000-0001-6879-321X

REFERENCES

1. Goldman LM, Twedt R, Balasubramanian S. ALON optical ceramic transparencies for window, dome, and transparent armor applications. Proc SPIE. 2011;8016(4):77.
2. Goldman LM, Balasubramanian S, Nagendra N, Smith M. ALON® optical ceramic transparencies for sensor and armor applications. Structure. 2012;380:700.
3. Hu WW, Zhu QQ, Hao LY, Xu X, Agathopoulos S. Luminescence properties and energy transfer in Al5O6N:Ce3+, Tb3+ phosphors. J Lumin. 2014;149(5):155–8.
4. Zhang F, Chen S, Chen JF, Zhang HL, Li J, Liu XJ, et al. Characterization and luminescence properties of AlON:Eu^{2+} phosphor for white-emitting-diode illumination. J Appl Phys. 2012;111(8):2001–928.
5. Kim YW, Park HC, Lee YB, Oh KD, Stevens R. Reaction sintering and microstructural development in the system Al_2O_3–AlN. J Eur Ceram Soc. 2001;21(13):2383–91.
6. Bandyopadhyay S, Rixecker G, Aldinger F, Pal S, Mukherjee K, Maiti HS. Effect of reaction parameters on γ-AlON formation from Al_2O_3 and AlN. J Am Ceram Soc. 2010;85(4):1010–2.
7. Su M, Zhou Y, Wang K, Yang Z, Cao Y, Hong M. Highly transparent AlON sintered from powder synthesized by direct nitridation. J Eur Ceram Soc. 2015;35(4):1173–8.
8. Zhang N, Liang B, Wang XY, Kan HM, Zhu KW, Zhao XJ. The pressureless sintering and mechanical properties of AlON ceramic. Mater Sci Eng, A. 2011;528(19–20):6259–62.
9. Rafaniello W, Cutler IB. Preparation of sinterable cubic aluminum oxynitride by the carbothermal nitridation of aluminum oxide. J Am Ceram Soc. 1981;64(10):C-128.
10. Hartnett TM, Gentilman RL, Maguire EA. Aluminum oxynitride having improved optical characteristics and method of manufacture. United States patent 4481300. 1984.
11. Martin C, Cales B. Synthesis and hot pressing of transparent aluminum oxynitride. Proc SPIE. 1989;1112:20–4.
12. Sun WZ, Chen YH. Sintering behavior and properties of γ-alon transparent ceramics prepared by hot press sintering. J Mater Sci Eng. 2015;33(6):145–9.
13. Zheng YT, Yun XF, Zhang XK. Fabrication and microstructure of AlON ceramic by self-propagating high-temperature synthesis and hot isostatic pressing. Mater Sci Technol. 2008;16(4):481–4.
14. Chen F, Zhang F, Wang J, Zhang H, Tian R, Zhang J, et al. Microstructure and optical properties of transparent aluminum oxynitride ceramics by hot isostatic pressing. Scr Mater. 2014;81(3):20–3.
15. Chen CF, Yang P, King G, Tegtmeier EL. Processing of transparent polycrystalline AlON:Ce^{3+} scintillators. J Am Ceram Soc. 2016;99(2):424–30.
16. Liu Q, Jiang N, Li J, Sun K, Pan Y, Guo J. Highly transparent AlON ceramics sintered from powder synthesized by carbothermal reduction nitridation. Ceram Int. 2016;42(7):8290–5.
17. Zhao J, Harmer MP. Effect of pore distribution on microstructure development: ii, first- and second-generation pores. J Am Ceram Soc. 2010;71(7):530–9.
18. Shi JL. Relations between coarsening and densification and mass transport path in solid-state sintering of ceramics: model analysis. J Mater Res. 1999;14(4):1378–88.
19. Rahimian M, Ehsani N, Parvin N, Baharvandi HR. The effect of particle size, sintering temperature and sintering time on the properties of Al–Al_2O_3 composites, made by powder metallurgy. J Mater Process Technol. 2009;209(14):5387–93.
20. Yeh TS, Sacks MD. Effect of particle size distribution on the sintering of alumina. J Am Ceram Soc. 2010;71(12):C-484–7.
21. Yoshida K, See CC, Yokoyama S, Yano T. Effects of SiC particle size and sintering temperature on microstructure of porous SiC ceramics based on in-situ grain growth. Ceram Eng Sci Proc. 2015;35(5):173–83.
22. Sathiyakumar M, Gnanam FD. Influence of milling liquids and additives on particle size reduction and sintering behaviour of Al_2O_3. Br Ceram Trans. 2002;101(5):200–7.

23. Shi JL, Deguchi Y, Sakabe Y. Relation between grain growth, densification and surface diffusion in solid state sintering—a direct observation. J Mater Sci. 2005;40(21):5711–9.
24. Shan Y, Xu J, Wang G, Sun X, Liu G, Xu J, et al. A fast pressureless sintering method for transparent AlON ceramics by using a bimodal particle size distribution powder. Ceram Int. 2015;41(3):3992–8.
25. Wang J, Fang Z, Feng C, Jian Z, Zhang H, Tian R, et al. Effect of Y_2O_3 and La_2O_3 on the sinterability of γ-AlON transparent ceramics. J Eur Ceram Soc. 2015;35(1):23–8.
26. Feng C, Fang Z, Wang J, Zhang H, Tian R, Zhao Z, et al. Hot isostatic pressing of transparent AlON ceramics with Y_2O_3/La_2O_3 additives. J Alloys Compd. 2015;650:753–7.
27. Jin X, Gao L, Sun J, Liu Y, Gui L. Highly transparent alon pressurelessly sintered from powder synthesized by a novel carbothermal nitridation method. J Am Ceram Soc. 2012;95(9):2801–7.
28. Wang J, Zhang F, Chen F, Zhang H, Tian R, Dong M, et al. Fabrication of aluminum oxynitride (γ-alon) transparent ceramics with modified gelcasting. J Am Ceram Soc. 2014;97(5):1353–5.
29. Kumar RS, Johnson R. Aqueous slip casting of transparent aluminum oxynitride. J Am Ceram Soc. 2016;99(10):3220–5.
30. Mccauley JW. A simple model for aluminum oxynitride spinels. J Am Ceram Soc. 2010;61(7–8):372–3.

How to cite this article: Feng Z, Qi J, Huang X, et al. Planetary ball-milling of AlON powder for highly transparent ceramics. *J Am Ceram Soc*. 2019;102:2377–2389. https://doi.org/10.1111/jace.16146